



# Emergent momentum scale, localization, and van Hove singularities in the graphene twist bilayer

S. Shallcross,<sup>1,\*</sup> S. Sharma,<sup>2</sup> and O. Pankratov<sup>1</sup>

<sup>1</sup>*Lehrstuhl für Theoretische Festkörperphysik, Staudstrasse 7-B2, 91058 Erlangen, Germany*

<sup>2</sup>*Max-Planck-Institut für Mikrostrukturphysik Weinberg 2, D-06120 Halle, Germany*

(Received 8 May 2012; revised manuscript received 5 March 2013; published 3 June 2013)

We identify an angle-dependent *momentum scale* as the fundamental property of a bilayer composed of mutually rotated graphene layers. The interlayer scattering processes at these characteristic momentum values define an effective Brillouin zone (a *Jones zone*) which, in general, differs from the Brillouin zone generated by the real-space lattice, which is physically irrelevant. From this we develop a numerical method that increases, for the twist bilayer, the efficiency of the standard tight-binding method by a factor of  $\approx 10^3$  at no loss of accuracy. The efficiency of the method is based on (i) the fact that the twist Hamiltonian is exceptionally sparse in a basis of single-layer graphene (SLG) states, (ii) a solution of trivial Diophantine problem (Bézout's identity) allows one to know in advance which matrix elements take nonzero values, and (iii) to access the electronic structure in a few electron volts about the Dirac point a truncated SLG basis consisting only of states in a somewhat larger energy window are required, leading to a much reduced size of the Hamiltonian. This allows a complete survey of the system which reveals (i) an angle-dependent series of van Hove singularities, (ii) an increasing mixing of SLG states as the twist angle is reduced leading to the appearance of localization of the twist bilayer wave functions at all energies in the small-angle limit, and (iii) a zero-energy peak in the density of states in an approximately self-similar small-angle regime.

DOI: [10.1103/PhysRevB.87.245403](https://doi.org/10.1103/PhysRevB.87.245403)

PACS number(s): 72.80.Vp, 73.20.At, 73.21.Ac, 73.22.Pr

## I. INTRODUCTION

Graphene layers with a mutual rotation present one of the richest manifestations of the physics of this remarkable material.<sup>1–14</sup> The crucial physical parameter is the rotation angle  $\theta$ , and the physical nature of the system depends strongly on the value of this angle. The physics of the twist bilayer includes at large angles a low-energy electronic decoupling of the layers, an angle-dependent Fermi velocity at intermediate angles, and a small-angle regime in which the electronic properties appear coupled to the emergence of a geometric moiré pattern in remarkable ways. New effects continue to be discovered, most recently the experimental identification of “missing states” in the quantum Hall effect, from which is inferred the existence of localized states, the origin of which is yet to be elucidated.<sup>15</sup>

Despite sustained investigation a clear theoretical understanding of this system has yet to emerge. There are two principal difficulties: (i) numerical calculation, and, hence, verification of approximate analytical theories, is impossible for the important small-angle case due to the diverging size of the unit cell and (ii) the applicability of Bloch's theorem is problematic; twist bilayer systems with very similar rotation angle, and, hence, very similar lattices and physical properties, may have wildly different translation symmetries. Theoretical progress therefore has mainly been driven by the development of effective low-energy theories, in which details of the lattice are dispensed with. These have been developed both for the large-<sup>6</sup> and small-angle<sup>1,8,13</sup> regimes. Among the key theoretical insights that have been obtained in this way are (i) the existence of a characteristic angle-dependent energy scale and a related suppression of the Fermi velocity for angles  $\theta < 15^\circ$ ,<sup>1</sup> (ii) the identification of a certain lattice symmetry, “sublattice exchange symmetry,”<sup>6</sup> and (iii) the derivation of a low-energy effective Hamiltonian in which the moiré length scale (see Fig. 1) plays a central role, from which follows the applicability of Bloch's theorem at low energies.<sup>8</sup>

In contrast to such approaches in this work we present a theory of the twist bilayer that retains the lattice, and, hence, is valid for *all energies*, but find that, remarkably, the lattice by itself vanishes from the theory. This occurs via the emergence of a characteristic momentum scale that depends only on the rotation angle of the bilayer and vanishes as  $\theta \rightarrow 0$  and that we identify as the fundamental physical property of this system. Near the Dirac point this is equivalent to the characteristic energy scale discussed in earlier works; however, away from the Dirac point it yields other energy scales that we demonstrate govern the generation of an angle-dependent series of high-energy van Hove singularities. Furthermore, the theory we deploy here yields (i) an explanation for the applicability of Bloch's theorem free from any approximations, and valid at all energies, and (ii) a numerical method as accurate as standard tight-binding calculations but several orders of magnitude faster. This numerical approach employs a basis of single-layer graphene states for the twist Hamiltonian that we show has two important properties: first, it leads to an exceptionally sparse structure for the twist Hamiltonian, allowing the deployment of an efficient Lanczos scheme for the diagonalization and, more importantly, we show that a solution to Bézout's identity (see Appendix), numerically trivial to obtain, allows one to know in advance which interlayer matrix elements take nonzero value. This avoids the evaluation of a huge number of negligible matrix elements, which themselves become numerically expensive in the small-angle limit.

With this numerical approach in hand we are able to provide a complete survey of the twist bilayer system, from large angles down to an approximately *self-similar* very small angle regime. In particular, we find that an increasing proportion of *all states* of the twist bilayer become localized as the rotation angle decreases, thus providing a possible explanation for the origin of the “missing states” in recent quantum Hall experiments.

The remainder of this article is structured as follows: we, first, present a lattice-based theory of the twist bilayer

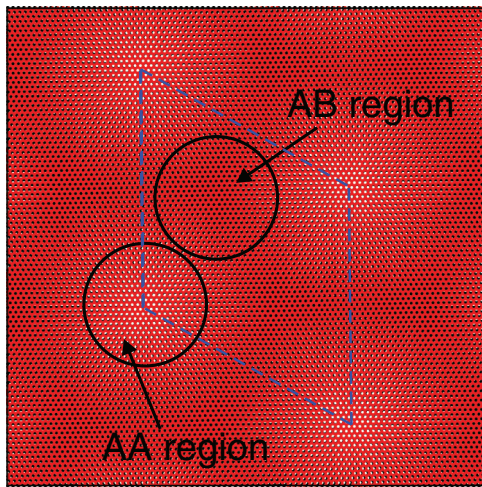


FIG. 1. (Color online) Twist bilayer with a mutual rotation of  $\theta = 1.20^\circ$  showing the emergence of a moiré lattice. Dashed lines indicate the real-space commensuration primitive cell; circles indicate regions of the lattice of AA and AB stacking. The moiré length  $D$  is defined as the separation between regions of AA (or AB) stacking and is here equal in length of the primitive vectors of the lattice.

that both explains the emergence of an angle-dependent momentum scale and underpins our numerical technique (Sec. II); subsequently, we provide details of the numerical technique itself (Sec. III, and Appendix); this is then followed by a section in which we explore the properties of the twist bilayer as a function of angle (Sec. IV), after which we conclude (Sec. V).

## II. THEORY

We first recall the basic geometry of the twist bilayer for the commensurate case. A number of equivalent formulations of this have been presented in the literature; here we follow that of Ref. 5. A unique commensuration geometry is generated by a co-prime integer pair  $(p, q)$  with a rotation angle given by  $\theta = \tan^{-1} [(3(q/p)^2 - 1)/(3(q/p)^2 + 1)]$ . These commensurations may be classified according to whether  $p$  is divisible by 3 and are conveniently labeled by the parameter  $\delta = 3/\text{gcd}(p, 3)$  (here gcd indicates the greatest common divisor). These two cases are related to the even and odd symmetry classes introduced in Ref. 6, although the precise correspondence between the parameter  $\delta$  and the symmetry class depends on the initial choice of rotation axis and stacking. The resulting commensuration vectors, i.e., the primitive vectors of the twist bilayer, are for the case  $\delta = 1$  given by

$$\mathbf{t}_1 = \frac{1}{\gamma} [-(p+3q)\mathbf{a}_1 - 2p\mathbf{a}_2], \quad (1)$$

$$\mathbf{t}_2 = \frac{1}{\gamma} [2p\mathbf{a}_1 - (p-3q)\mathbf{a}_2], \quad (2)$$

and for  $\delta = 3$  by

$$\mathbf{t}_1 = \frac{1}{\gamma} [-(p+q)\mathbf{a}_1 + 2q\mathbf{a}_2], \quad (3)$$

$$\mathbf{t}_2 = \frac{1}{\gamma} [-2q\mathbf{a}_1 - (p-q)\mathbf{a}_2], \quad (4)$$

where  $\gamma = \text{gcd}(p+3q, p-3q)$ , and  $\mathbf{a}_{1,2}$  are the lattice vectors of the unrotated graphene cell. Evidently, there exists a “many-to-one” relation between the rotation angle, which may be expressed as a function of  $q/p$ , and the lattice vectors  $\mathbf{t}_{1,2}$ , which depend on  $p, q$  separately. On the other hand, the emergent moiré lattice that is found for  $\theta \lesssim 15^\circ$  depends *only on the rotation angle*  $\theta$  through the moiré length  $D = \frac{a}{2\sin\theta/2}$ , where  $a$  is the lattice parameter (see Fig. 1).

To investigate electronic properties of this complex geometry we follow Ref. 5 and consider the twist bilayer potential to be a superposition of that of each separate layer, i.e.,  $V_B = V^{(1)} + V^{(2)}$  with the superscript a layer index, and as a basis set for the Hamiltonian take the direct product of the single-layer graphene (SLG) eigenstates from each layer. That is, for a given  $\mathbf{k}$  vector  $\mathbf{k}$  in the bilayer Brillouin zone (BZ), the appropriate basis elements comprise the set of SLG eigenstates from layer 1 (2)  $\{|\phi_{i_1 k_1}^{(1)}\rangle\}$  ( $\{|\phi_{i_2 k_2}^{(2)}\rangle\}$ ) that satisfy

$$\mathbf{k}_{1(2)} = \mathbf{k} + \alpha_{1(2)}\mathbf{g}_1 + \beta_{1(2)}\mathbf{g}_2, \quad (5)$$

with  $\mathbf{g}_{1,2}$  the reciprocal lattice vectors of the twist bilayer and  $\alpha_{1(2)}, \beta_{1(2)}$  integers such that  $\mathbf{k}_{1(2)}$  falls in the Brillouin zone of layer 1 (2). Here we have introduced a notation for SLG eigenstates that we follow throughout this article:  $|\phi_{i_n k_n}^{(n)}\rangle$  represents a SLG eigenstate from layer  $n$ , and  $i_n$  and  $\mathbf{k}_n$  label a state and  $\mathbf{k}$ -vector index, respectively. This basis set is, evidently, nothing more than the usual “folding back” condition encountered in superlattice geometries. Nevertheless, it already serves to illustrate the essential difficulty in dealing with this system from a lattice-based perspective. To that end we recall<sup>5</sup> that the bilayer reciprocal lattice vectors are, for  $\delta = 1$ , given by

$$\mathbf{g}_1 = \frac{\gamma}{3(p^2 + 3q^2)} [(p+3q)\mathbf{b}_1 + 2p\mathbf{b}_2] \quad (6)$$

$$\mathbf{g}_2 = \frac{\gamma}{3(p^2 + 3q^2)} [-2p\mathbf{b}_1 - (p-3q)\mathbf{b}_2],$$

and for  $\delta = 3$  by

$$\mathbf{g}_1 = \frac{\gamma}{p^2 + 3q^2} [-(p-q)\mathbf{b}_1 + 2q\mathbf{b}_2] \quad (7)$$

$$\mathbf{g}_2 = \frac{\gamma}{p^2 + 3q^2} [-2q\mathbf{b}_1 - (p+q)\mathbf{b}_2],$$

where  $\mathbf{b}_{1,2}$  are the standard reciprocal lattice vectors of the unrotated graphene lattice and, like their real-space counterparts  $\mathbf{t}_{1,2}$ , depend on  $p, q$  separately. There thus exists a many-to-one relation between  $\mathbf{g}_{1,2}$  and the rotation angle. However, as the  $\mathbf{g}_{1,2}$  determine which SLG states may be coupled by the interlayer interaction (via the folding back procedure), it then appears as if the bilayer electronic structure has *no dependence on rotation angle*: a paradoxical situation. This is the essence of the problem in application of Bloch’s theorem to this system.

To resolve this breakdown in the naive application of lattice physics we, first, notice that in the basis outlined above the twist bilayer Hamiltonian assumes a convenient  $2 \times 2$  structure in layer space: layer diagonal blocks that contain only single-layer information and *layer off-diagonal blocks* which describe the interlayer coupling and consist of elements of the form  $\langle \phi_{i_1 k_1}^{(1)} | V_B | \phi_{i_2 k_2}^{(2)} \rangle$ . Evidently, such matrix elements are of *mixed translational symmetry*, that is, are composed of objects possessing the translational symmetry of SLG, as well

as objects possessing the translation symmetry of rotated SLG. If we then insert a Fourier expansion for each of these we find

$$\langle \phi_{i_1 \mathbf{k}_1}^{(1)} | V_B | \phi_{i_2 \mathbf{k}_2}^{(2)} \rangle = \sum_{\mathbf{G}_1, \mathbf{R}\mathbf{G}_2} C_{i_1 \mathbf{k}_1 + \mathbf{G}_1}^{i_2 \mathbf{k}_2 + \mathbf{R}\mathbf{G}_2} \delta_{\mathbf{G}_1 = \mathbf{R}\mathbf{G}_2 + \mathbf{k}_2 - \mathbf{k}_1}, \quad (8)$$

where the sets  $\{\mathbf{G}_1\}$  ( $\{\mathbf{R}\mathbf{G}_2\}$ ) consist of reciprocal lattice vectors of SLG (rotated SLG). As stressed in Ref. 5, the advantage of this approach is that the interlayer matrix elements have been split into an electronic part, the  $C_{i_1 \mathbf{k}_1 + \mathbf{G}_1}^{i_2 \mathbf{k}_2 + \mathbf{R}\mathbf{G}_2}$  and a *purely geometric* term  $\delta_{\mathbf{G}_1 = \mathbf{R}\mathbf{G}_2 + \mathbf{k}_2 - \mathbf{k}_1}$ . This represents an interlayer momentum conservation condition (a selection rule) and only terms for which

$$\mathbf{G}_1 = \mathbf{R}\mathbf{G}_2 + \mathbf{k}_2 - \mathbf{k}_1 \quad (9)$$

contribute to the matrix element sum. The solutions of this equation may be visualized as the set of coincident points between the reciprocal lattice of SLG and the reciprocal lattice of rotated SLG, with an additional shift of  $\mathbf{k}_2 - \mathbf{k}_1$  applied to the latter. Interestingly, then, the electronic structure of the twisted bilayer leads to a *reciprocal space analog* of the real-space commensuration condition for the existence of a (periodic) lattice. A crucial difference from the real-space commensuration problem is the term  $\mathbf{k}_2 - \mathbf{k}_1$ , and this results in the reciprocal space commensuration lattice being shifted off the  $\Gamma$  point by some vector  $\Delta\mathbf{G}$ , as illustrated in Fig. 2. One might intuitively expect that different  $\mathbf{k}_2 - \mathbf{k}_1$  in Eq. (9) will lead to different shifts  $\Delta\mathbf{G}$  of the *same* commensuration lattice (i.e., a commensuration lattice with identical primitive vectors). This is indeed the case, and the proof of this we give in Appendix. To draw out further the separation between electronic and geometric aspects of the interlayer matrix element, we note that the Fourier components  $C_{i_1 \mathbf{k}_1 + \mathbf{G}_1}^{i_2 \mathbf{k}_2 + \mathbf{R}\mathbf{G}_2}$  are expected to decrease with increasing magnitude of  $\mathbf{G}_1$  and  $\mathbf{R}\mathbf{G}_2$  (due to the smoothness of the bilayer potential in real space). Now the magnitude of the *smallest* contributing  $\mathbf{G}_1$  and  $\mathbf{R}\mathbf{G}_2$  as *allowed by the selection rule* Eq. (9) is evidently

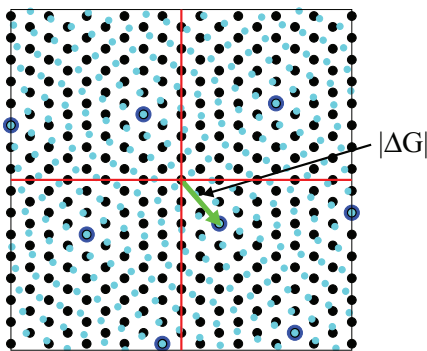


FIG. 2. (Color online) Reciprocal space analog of the real-space commensuration geometry. Any interlayer matrix element of the bilayer potential and single-layer graphene states,  $\langle \phi_{i_1 \mathbf{k}_1}^{(1)} | V_B | \phi_{i_2 \mathbf{k}_2}^{(2)} \rangle$ , leads to a reciprocal space commensuration between the unrotated SLG reciprocal lattice (black filled circles) and the rotated SLG reciprocal lattice *shifted by*  $\mathbf{k}_2 - \mathbf{k}_1$  (light filled circles). Only coincident points between these two lattices (large circles) contribute to the matrix element, which depends strongly on the shift of this coincident lattice off the origin, indicated by the arrow  $|\Delta\mathbf{G}|$ , see Fig. 3 and Sec. II for details.

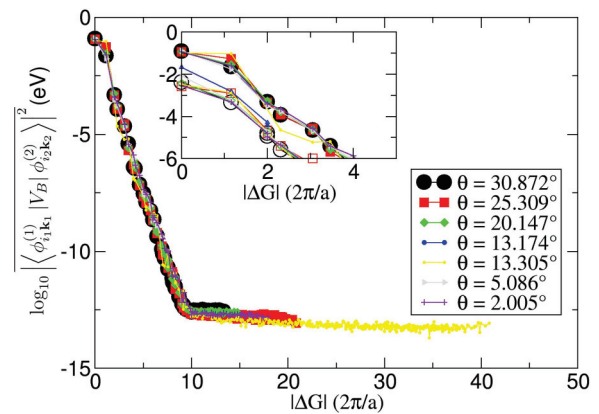


FIG. 3. (Color online) Main plot displays the logarithm of the averaged interlayer coupling matrix element  $\log_{10} |\langle \phi_{i_1 \mathbf{k}_1}^{(1)} | V_B | \phi_{i_2 \mathbf{k}_2}^{(2)} \rangle|^2$ , plotted as a function of the shift  $|\Delta\mathbf{G}|$  for several rotation angles. The quantity  $|\Delta\mathbf{G}|$  is the shift off the origin of a reciprocal space commensuration lattice that results from a Fourier analysis of the matrix element, see Sec. II for details. Evidently matrix elements for which  $|\Delta\mathbf{G}| > 4$  are effectively zero, and the corresponding single-layer states, are *not coupled by the bilayer potential*. The average is taken over the set of matrix elements for which the (single-layer graphene)  $\mathbf{k}$  vectors  $\mathbf{k}_1$  and  $\mathbf{k}_2$  generate the *same* shift term  $|\Delta\mathbf{G}|$  and where  $\mathbf{k}_1$  and  $\mathbf{k}_2$  run over all  $\mathbf{k}$  vectors in the unrotated and rotated Brillouin zones that fold back to the  $K$  point of the bilayer Brillouin zone; a similar result is found for any choice of  $\mathbf{k}$  vector in the bilayer Brillouin zone. The inset displays the region of the main graph for which the average of the matrix elements is less than  $10^{-6}$  and where the open symbols represent the standard deviation of the ensemble of matrix elements for which the average is computed.

determined by the magnitude of  $\Delta\mathbf{G}$ . We thus conclude that the magnitude of the interlayer matrix elements themselves should show a marked decrease with increasing  $|\Delta\mathbf{G}|$ .

To confirm this dependence a numerical investigation is required, and to that end we average over all matrix elements in the bilayer Hamiltonian for which the difference of the basis momenta  $\mathbf{k}_2 - \mathbf{k}_1$  yields a specific value of  $|\Delta\mathbf{G}|$  and then plot this average as a function of  $|\Delta\mathbf{G}|$ , as shown in Fig. 3. To evaluate the interlayer matrix elements we use the tight-binding method recently deployed to study graphene twist flakes; see Ref. 16 for details of this. To determine the  $|\Delta\mathbf{G}|$  for each matrix element we solve Eq. (9) numerically, as described in Appendix. The set of matrix elements that we use to determine the averages shown in Fig. 3 consists of all interlayer matrix elements in the bilayer Hamiltonian evaluated at the  $K$  point in the bilayer Brillouin zone. Virtually identical results are obtained for any choice of  $\mathbf{k}$  vector. A number of points may immediately be noted from Fig. 3: (i) the average matrix element decays with increasing shift  $|\Delta\mathbf{G}|$ , and this decay is in fact exponential; (ii) already by  $|\Delta\mathbf{G}| = 3$  the magnitude is reduced by four orders as compared to the value for  $|\Delta\mathbf{G}| = 0$ ; and (iii) the form of the decay is not very sensitive to rotation angle. (Note that here, and subsequently throughout this article, we present all reciprocal space quantities in units of  $2\pi/a$ . Similarly, all quantities in real space will be presented in units of  $a$ , with  $a$  the graphene lattice parameter.)

From this analysis we conclude that all matrix elements for which  $|\Delta\mathbf{G}| > 4$  are effectively zero and single-layer

graphene states for which the momenta difference  $\mathbf{k}_2 - \mathbf{k}_1$  leads to  $|\Delta\mathbf{G}|$  greater than this value *are not coupled by the bilayer potential*. It thus is not the electronic  $C_{i,\mathbf{k}_1+\mathbf{G}_1}^{i_2\mathbf{k}_2+\mathbf{R}\mathbf{G}_2}$  that are important for understanding the interlayer interaction but the geometric selection rule Eq. (9). The physics of the interlayer interaction is evidently determined by which  $\mathbf{k}_2 - \mathbf{k}_1$  lead to  $|\Delta\mathbf{G}| < 4$  and to address this problem we must now consider explicit solutions to Eq. (9).

The solution set  $\{\mathbf{G}_1\}$  of Eq. (9), expressed as  $\mathbf{G}_1 = m_1\mathbf{b}_1 + m_2\mathbf{b}_2$ , is for the case  $\delta = 1$  given by

$$\begin{pmatrix} m_1 \\ m_2 \end{pmatrix} = \alpha \begin{pmatrix} p+3q \\ 2p \end{pmatrix} + \beta \begin{pmatrix} -2p \\ -p+3q \end{pmatrix} + \frac{\gamma}{6p} \begin{pmatrix} l_1-2l_2 \\ 2l_1-l_2 \end{pmatrix} \quad (10)$$

and for  $\delta = 3$  by

$$\begin{pmatrix} m_1 \\ m_2 \end{pmatrix} = \alpha \begin{pmatrix} -p+q \\ 2q \end{pmatrix} + \beta \begin{pmatrix} 2q \\ p+q \end{pmatrix} - \frac{\gamma}{2p} \begin{pmatrix} l_1 \\ l_2 \end{pmatrix} \quad (11)$$

(see Ref. 5 and also Appendix), where  $\alpha, \beta$  are integers and  $l_{1,2}$  the coefficients which arise when the SLG  $\mathbf{k}$ -vector difference  $\mathbf{k}_2 - \mathbf{k}_1$  is expressed in terms of the bilayer reciprocal lattice vectors:  $\mathbf{k}_2 - \mathbf{k}_1 = l_1\mathbf{g}_1 + l_2\mathbf{g}_2$ .

From these equations we see that when

$$\mathbf{k}_2 - \mathbf{k}_1 = n_1\mathbf{g}_1^{(c)} + n_2\mathbf{g}_2^{(c)} \quad (12)$$

with  $n_{1,2}$  integers, and where the *coupling vectors*  $\mathbf{g}_{1,2}^{(c)}$  are defined by

$$\mathbf{g}_1^{(c)} = -\frac{2p}{\gamma}(\mathbf{g}_1 + 2\mathbf{g}_2) \quad \mathbf{g}_2^{(c)} = \frac{2p}{\gamma}(2\mathbf{g}_1 + \mathbf{g}_2) \quad (13)$$

for the case when  $\delta = 1$  and

$$\mathbf{g}_1^{(c)} = -\frac{2p}{\gamma}\mathbf{g}_1 \quad \mathbf{g}_2^{(c)} = -\frac{2p}{\gamma}\mathbf{g}_2 \quad (14)$$

for the case  $\delta = 3$ , the shift  $\Delta\mathbf{G}$  then is given by

$$\Delta\mathbf{G} = n_1\mathbf{b}_1 + n_2\mathbf{b}_2. \quad (15)$$

This may be seen directly by the substitution of Eqs. (12) and (13) into Eq. (10) or Eqs. (12) and (14) into Eq. (11). We thus see that it is only when the difference of the single-layer momenta  $\mathbf{k}_2 - \mathbf{k}_1$  is given by a low-integer multiple of the coupling momenta vectors will the resulting interlayer matrix element be nonzero; all *other* matrix elements belong to the extended ‘‘tail’’ of Fig. 3.

Therefore, it is these vectors which, as far as the electronic properties of the twist bilayer are concerned, *are the only relevant reciprocal space vectors*. The interlayer conservation of momentum ensures that the usual *geometric* reciprocal space vectors  $\mathbf{g}_{1,2}$  are physically irrelevant and, therefore, the bilayer Brillouin zone constructed from  $\mathbf{g}_{1,2}$  is also physically irrelevant. The physical reciprocal space primitive cell is instead that constructed from the coupling vectors  $\mathbf{g}_{1,2}^{(c)}$ .<sup>17</sup> Finally, we note that from Eq. (13) we have  $g^{(c)} = |\mathbf{g}_{1,2}^{(c)}| = \frac{2p}{\gamma}\sqrt{3}g$ , and similarly from Eq. (14)  $g^{(c)} = \frac{2p}{\gamma}g$ , where  $g = |\mathbf{g}_{1,2}|$ . On the other hand, from the formulas for the rotation angle and  $\mathbf{g}_{1,2}$  given above, one finds  $g = \frac{2\gamma}{3p}\sin\theta/2$  (for  $\delta = 1$ ) and  $g = \frac{2\gamma}{\sqrt{3}p}\sin\theta/2$  (for  $\delta = 3$ ). Combining these results for  $g^{(c)}$

and  $g$  then immediately yields

$$g^{(c)} = \frac{4}{\sqrt{3}}\sin\frac{\theta}{2}, \quad (16)$$

which is independent of the lattice parameters  $\gamma, \delta, p, q$ . We thus see that the momentum scale on which single-layer graphene states are coupled by the bilayer interaction depends *only on the rotation angle*. The lattice has ‘‘vanished by itself,’’ without recourse to any additional (e.g., low-energy or continuum) approximation. Interestingly, this momentum scale is exactly that which corresponds to the real-space moiré length scale  $D = \frac{1}{2\sin\theta/2}$ ; the magnitude of the reciprocal lattice vectors for a hexagonal lattice of lattice parameter  $D$  (i.e., the moiré lattice) is exactly equal to  $g^{(c)}$ .

To illustrate this for a specific example we consider a twist bilayer for which  $(p, q) = (1, 5)$ , corresponding to a rotation angle of  $\theta = 13.174^\circ$ . We note that for this commensuration geometry  $\delta = 3/\text{gcd}(p, 3) = 1$  and  $\gamma = \text{gcd}(3q + p, 3q - p) = 2$ , and, hence, from Eq. (14) we find that  $\mathbf{g}_{1,2}^{(c)} = \mathbf{g}_{1,2}$ . This equality of the coupling reciprocal vectors and their geometric counterparts occurs whenever the real-space unit cell is equal in area to the moiré unit cell; this occurs when  $(p = 1, q \in \{\text{odd integers}\})$ . We now consider a number of lattices that have angles very close to that of the  $(p, q) = (1, 5)$  case but, necessarily, primitive cells containing a greatly increased number of carbon atoms  $N$  and, therefore, reciprocal lattice vectors  $\mathbf{g}_{1,2}$  greatly decreased in magnitude from the  $(p, q) = (1, 5)$  case. This leads to a proliferation of SLG states that may, in principle, be coupled by the interlayer interaction. In Fig. 4 we present density plots of  $|\Delta\mathbf{G}|$  that are obtained by fixing  $\mathbf{k}_1$  at the point labeled  $A$  in these figures and then allowing  $\mathbf{k}_2$  to run over all  $\mathbf{k}$  vectors in the rotated BZ such that  $\mathbf{k}_2 = \mathbf{k}_1 + \alpha\mathbf{g}_1 + \beta\mathbf{g}_2$  (where as usual  $\alpha, \beta$  represent integers); Eq. (9) is then solved numerically to find  $|\Delta\mathbf{G}|$  for the given  $\mathbf{k}_2 - \mathbf{k}_1$ . In this figure one can strikingly see that while the details of the function  $|\Delta\mathbf{G}|$  are lattice dependent, there is the emergence of a structure that is governed entirely by the coupling vectors  $\mathbf{g}_{1,2}^{(c)}$  and, hence, depends *only on the rotation angle*.

To relate this structure more closely to the  $\mathbf{g}_{1,2}^{(c)}$  we present in Fig. 5  $|\Delta\mathbf{G}|$  plotted along the line sections marked  $AB$  in Fig. 4. One observes, first, that  $|\Delta\mathbf{G}|$  is a complex function of  $\mathbf{k}_2 - \mathbf{k}_1$  and differs markedly for different  $N$  generated by very similar rotation angles. However, these line sections, as may be seen from Fig. 5, all include  $\mathbf{k}_2 - \mathbf{k}_1 = n_2\mathbf{g}_2^{(c)}$  for  $n_2 = \{0, -1, -2\}$  and, as may be seen from the inset of Fig. 5, the  $\Delta\mathbf{G}$  generated by these  $\mathbf{k}$ -vector differences are (i) identical for each  $N$  and (ii) correspond to the minimum  $\Delta\mathbf{G}$  on the line section. (The small changes arise from the fact that the set of rotation angles chosen are close but obviously not identical.) To investigate the impact of this structure of  $|\Delta\mathbf{G}|$  on the electronic properties we plot in Fig. 6 the interlayer matrix element  $|\langle\phi_{i_1\mathbf{k}_1}^{(1)}|V_B|\phi_{i_2\mathbf{k}_2}^{(2)}\rangle|^2$  over the same line section. Evidently only those SLG states that are connected by the coupling vectors assume a nonzero value, as expected from the preceding discussion. In addition, one notes that the interlayer matrix elements decay exponentially with  $\mathbf{g}_2^{(c)}$ , a consequence of the exponential decay of all interlayer matrix elements with  $|\Delta\mathbf{G}|$ .

Finally, it is interesting to note that the only two ingredients that have been used in this derivation are (i) misorientation

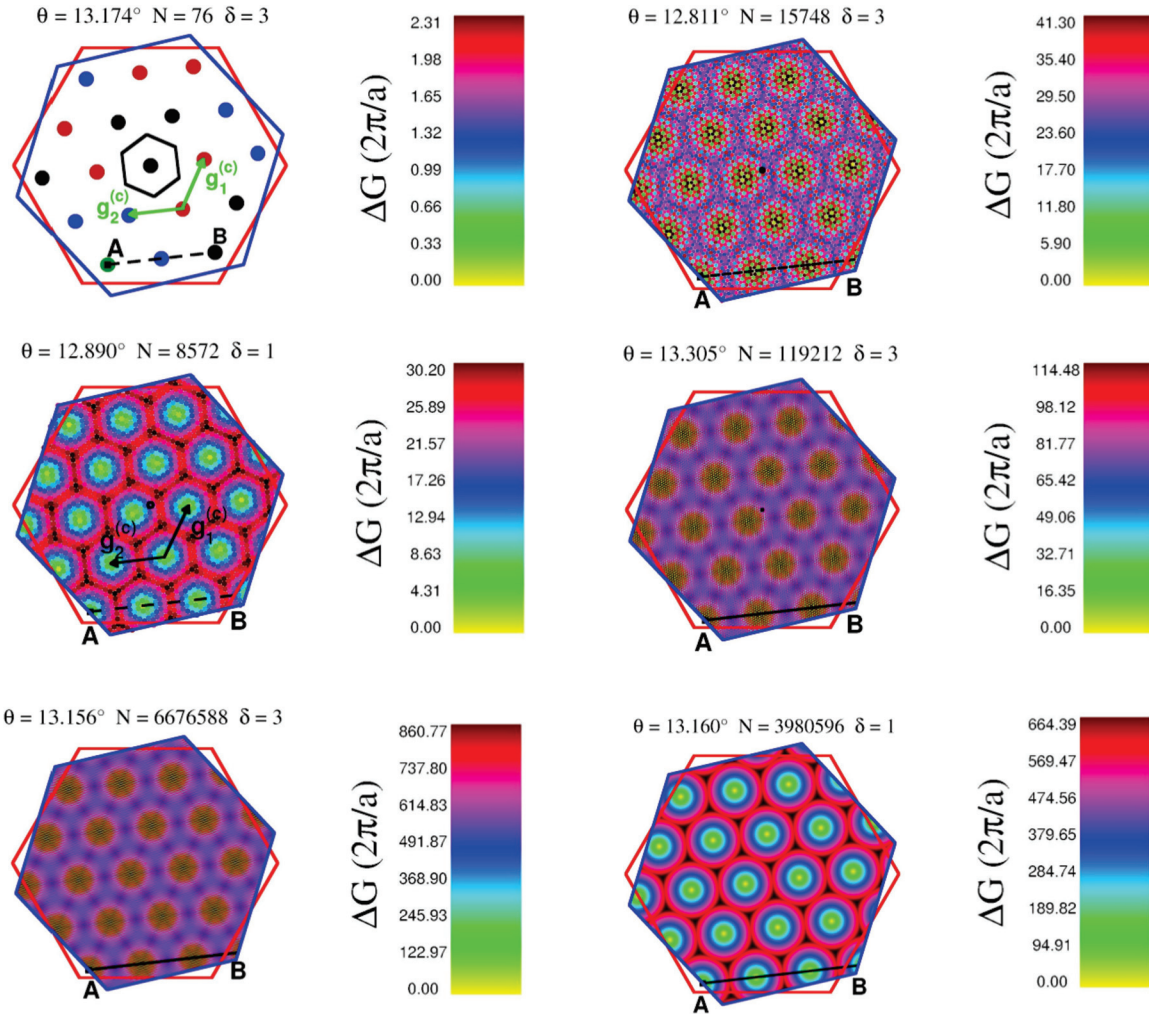


FIG. 4. (Color online) Momentum-space counterparty to the real-space moiré lattice: density plot of the magnitude of the shift term  $|\Delta\mathbf{G}|$  that determines the magnitude of interlayer matrix elements  $\langle\phi_{i_1\mathbf{k}_1}^{(1)}|V_B|\phi_{i_2\mathbf{k}_2}^{(2)}\rangle$ ; only matrix elements for which  $|\Delta\mathbf{G}| < 4$  assume a nonzero value. See Fig. 3 and Sec. II for details. In these plots  $\mathbf{k}_1$  is fixed to the point labeled A and all  $\mathbf{k}_2$  that interact with  $\mathbf{k}_1$  are shown (interaction is allowed if the difference of these momenta are integer valued in terms of the bilayer reciprocal lattice vectors). Shown are results for a set of very similar angles that, necessarily, correspond to very different real-space primitive cell sizes:  $N$  is the number of atoms in the primitive cell. While details of  $|\Delta\mathbf{G}|$  evidently depend on details of the real-space primitive cell geometry, one observes an emergent structure that is independent of  $N$  and depends only on the rotation angle  $\theta$  through the coupling momentum scale  $g^{(c)} = |\mathbf{g}_{1,2}^{(c)}|$ . The point labeled B describes the line section on which  $|\Delta\mathbf{G}|$  and  $\langle\phi_{i_1\mathbf{k}_1}^{(1)}|V_B|\phi_{i_2\mathbf{k}_2}^{(2)}\rangle$  are plotted in Figs. 5 and 6, respectively.

of identical layers and (ii) a sufficiently fast decay of the coefficients of the Fourier expansions. The theoretical approach outlined above (and the numerical methods that derive from it, as outlined in the subsequent section) are, thus, more general than their specific application to the graphene honeycomb lattice.

### III. NUMERICAL METHOD

From the analysis of the previous section it is clear that, when expressed in the SLG basis, the twist bilayer Hamiltonian assumes a sparse structure. This is due to the fact that (i) when  $\mathbf{k}_2 - \mathbf{k}_1 \neq n_1\mathbf{g}_1^{(c)} + n_2\mathbf{g}_2^{(c)}$  the interlayer matrix element  $\langle\phi_{i_1\mathbf{k}_1}^{(1)}|V_B|\phi_{i_2\mathbf{k}_2}^{(2)}\rangle$  is negligible and (ii) such matrix elements decrease exponentially with  $n_{1,2}$ . In addition, the layer diagonal blocks are diagonal in state indices  $i_1\mathbf{k}_1$  and consist simply of the single-layer graphene eigenvalues  $\epsilon_{i_1\mathbf{k}_1}$ . This

follows as we have  $\langle\phi_{i_1\mathbf{k}_1}^{(n)}|V_B|\phi_{i_2\mathbf{k}_2}^{(n)}\rangle = \epsilon_{i_1\mathbf{k}_1}\delta_{i_1\mathbf{k}_1,i_2\mathbf{k}_2}$  due to the orthogonality of SLG states and the fact that  $\langle\phi_{i_1\mathbf{k}_1}^{(1)}|V_2|\phi_{i_2\mathbf{k}_2}^{(1)}\rangle = \langle\phi_{i_1\mathbf{k}_1}^{(2)}|V_1|\phi_{i_2\mathbf{k}_2}^{(2)}\rangle = 0$  as these terms correspond to three-center hopping integrals that are identically zero in the tight-binding method we deploy here (and are quite generally negligible).

This exceptionally sparse structure allows the deployment of a Lanczos technique that greatly reduces the numerical cost of diagonalization.<sup>18</sup> This fact, however, is only partly responsible for the efficiency of the algorithm we propose here, and there are two further crucial points that account for the numerical efficiency.

First, the calculation of matrix elements of the form  $\langle\phi_{i_1\mathbf{k}_1}^{(1)}|V_B|\phi_{i_2\mathbf{k}_2}^{(2)}\rangle$  is, in the small-angle limit especially, numerically rather expensive as it involves sums over the number of carbon atoms  $N$  in the real-space primitive cell. However, for any matrix element  $\langle\phi_{i_1\mathbf{k}_1}^{(1)}|V_B|\phi_{i_2\mathbf{k}_2}^{(2)}\rangle$  we may determine the

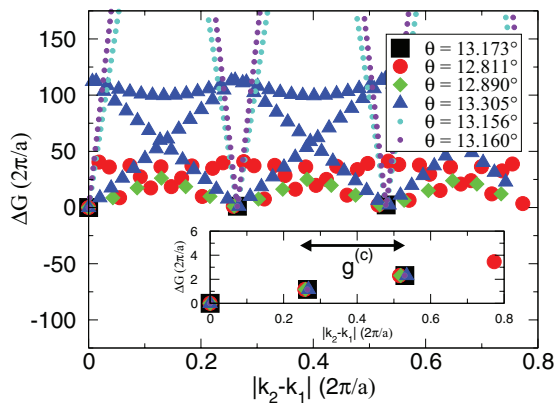


FIG. 5. (Color online) The shift term  $|\Delta\mathbf{G}|$  plotted on the line section  $AB$  in the rotated Brillouin zone indicated in Fig. 4. The inset shows the minimum values of  $|\Delta\mathbf{G}|$  that are given by Eqs. (12), (13), and (14). These occur when the momentum difference between the single-layer graphene states  $\mathbf{k}_2 - \mathbf{k}_1$  takes on values of  $-n_2\mathbf{g}_2$  with  $n_2 = \{0, -1, -2\}$ ; see also Fig. 4.

shift  $|\Delta\mathbf{G}|$  from Eq. (9), which may be numerically solved for arbitrary  $\mathbf{k}_2 - \mathbf{k}_1$  using the extended Euclid algorithm as outlined in Appendix. As the extended Euclid algorithm employs at most  $5h$  integer algebra steps, where  $h$  is the number of base-10 digits in the smaller of  $p$  and  $q$  (see Ref. 19), the calculation of  $|\Delta\mathbf{G}|$  is of negligible cost in comparison to the calculation of matrix elements. The twist bilayer Hamiltonian thus may be very efficiently constructed with recourse to Euclid's algorithm; only those matrix elements for which  $|\Delta\mathbf{G}| < \Delta G_{\max}$  are calculated. We find that to accurately reproduce results for the exact tight-binding method  $\Delta G_{\max} = 3$  is sufficient.

A second reason is that if we wish to evaluate the twist bilayer electronic structure in some energy window  $(E_1, E_2)$ , we require only SLG eigenstates in a somewhat greater energy window, which we find from numerical experience to be

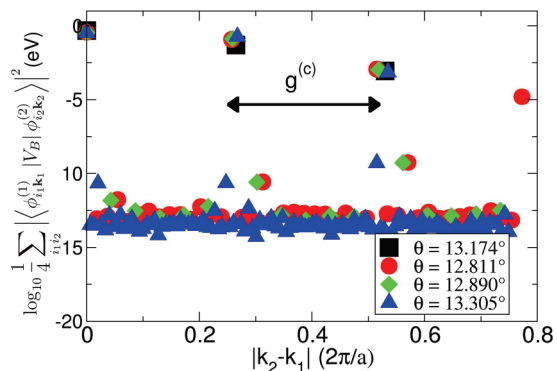


FIG. 6. (Color online) The interlayer matrix element  $|\langle \phi_{i_1 k_1}^{(1)} | V_B | \phi_{i_2 k_2}^{(2)} \rangle|^2$  averaged over the SLG graphene band index  $(i_1, i_2 = 1, 2)$  and plotted on the line section indicated in Fig. 4. Note that only when the momentum difference of the SLG states, i.e., when the difference of the  $\mathbf{k}$ -vector labels  $\mathbf{k}_2 - \mathbf{k}_1$ , is an integer multiple of the coupling momenta  $\mathbf{g}_{1,2}^{(c)}$  are the two states coupled by the interlayer interaction. In the particular case shown this occurs when  $\mathbf{k}_2 - \mathbf{k}_1 = -n_2\mathbf{g}_2$  and, hence, all points in the graph are separated by  $g^{(c)} = |\mathbf{g}_{1,2}^{(c)}|$ .

approximately given by  $(1.5E_1, 1.5E_2)$ . The underlying reason for this is that the bilayer potential is rather weak; SLG eigenstates very far in energy from the window of interest are not coupled by this weak potential. As we are often only interested in an energy window of a few electron volts about the Dirac point, this allows for a substantial truncation of the bilayer Hamiltonian when expressed in the SLG basis.

Properties such as the density of states and layer- or site-projected density of states are then obtained from the eigenvalues in a standard way (note that to obtain projections one needs to transform the eigenstates from the SLG basis back to a real-space basis). Using this approach (that we estimate is of the order of  $10^3$  times faster than the standard tight-binding method at small angles), we can completely survey the electronic structure as a function of twist angle.

#### IV. RESULTS

Figures 7(a)–7(i) show the density of states (DOS) as a function of angle, plotted in the energy range  $-3$  to  $2$  eV. Three salient features may be noted: (i) the SLG van Hove singularity (vHS) at  $-2.2$  eV is split into an increasing number of distinct high-energy vHS's as the twist angle is reduced; (ii) the energy window between the low-energy vHS's, indicated by  $\Delta_1$  [see Fig. 7(b)], reduces as the twist angle is reduced (this is the window in which decoupled SLG cones may be found); nevertheless, (iii) in the small-angle

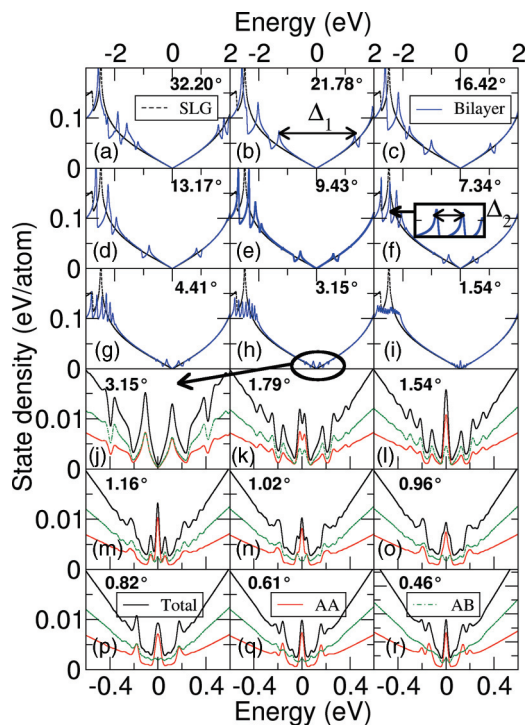


FIG. 7. (Color online) Total density of states (DOS) of the twist bilayer for angles between  $32.20^\circ$  and  $0.46^\circ$  calculated using the efficient tight-binding method described in the text. AA-DOS and AB-DOS indicate the DOS projected onto these regions of the moiré lattice (see Fig. 4 for illustration of the relation of these regions to the bilayer unit cell); in panels (a)–(i) the dashed line indicates the DOS of single-layer graphene. Note that panels (a)–(i) use the upper energy scale, while panels (j)–(r) the lower energy scale.

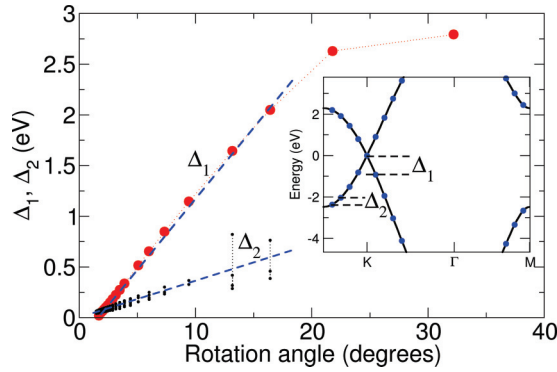


FIG. 8. (Color online) Dirac cone window  $\Delta_1$  (given by the separation of the *low-energy* van Hove singularities), indicated by large filled circles, and the *high-energy* van Hove singularity separations  $\Delta_2$ , indicated by small filled circles, plotted versus the twist bilayer rotation angle  $\theta$ . (Inset) The origin of *multiple energy scales* in the density of states via the coupling of SLG states by a *single momentum scale*; see text for details.

limit apart from the “smearing” of the  $-2.2$  eV SLG vHS into a multitude of peaks, and a residual structure near the Dirac point, the low-angle-state density is almost coincident with that of SLG. In summary, the development of the DOS with angle can be understood as the “pushing” of an increasing number of vHS peaks to either the energy of the SLG  $M$  point vHS peak at  $-2.38$  eV or to the Dirac point. As the twist angle approaches zero these low-energy vHS separated by  $\Delta_1$  ultimately merge into a pronounced peak in the DOS centered at zero energy, as shown in Figs. 7(j)–7(r). Note that at these small angles [see Figs. 7(o)–7(r)] the DOS changes very little, and so the system is approximately self-similar at these angles. In approximate analytical theories, valid in the small-angle regime, this low-energy peak in the DOS emerges as the zero mode of a non-Abelian moiré potential;<sup>14</sup> in the complete picture presented here we see that it represents the low-energy and low-angle limit of the vHS’s present at *all angles*.

The energy scales of the low- and high-energy vHS’s,  $\Delta_1$  and  $\Delta_2$  respectively [see Figs. 7(b) and 7(f)], clearly show

a different but, for  $\theta < 15^\circ$ , linear dependence on  $\theta$  (see Fig. 8). In fact, this result follows directly from the existence of a universal momentum scale  $g^{(c)}$  by which SLG eigenstates couple: we have  $\Delta_1 = v(\epsilon = 0 \text{ eV})g^{(c)}$  and  $\Delta_2 = v(\epsilon = -2.38 \text{ eV})g^{(c)}$  with  $v(\epsilon)$  the band velocity at energy  $\epsilon$ . This is illustrated in the inset of Fig. 8. In this case, we expect the ratio  $\Delta_1/\Delta_2$  to match the ratio of the band velocities and indeed numerically this is the case:  $v(0.00\text{eV})/v(-2.38\text{eV}) = 0.236$  and  $\Delta_1/\Delta_2 = 0.243$ . Note that the linearity of  $\Delta_{1,2}$  follows from the small-angle expansion of the  $\sin(\theta/2)$  in  $g^{(c)}$ . A close inspection of  $\Delta_1$  in Fig. 8 shows that the “best fit” line appears not to intercept the origin, in contrast to best fit line through the  $\Delta_2$  results. The origin of this behavior is the fact that at  $\approx 2^\circ$  the two peaks that constitute the end points of the energy separation  $\Delta_1$  merge into the single zero mode peak, as shown in Figs. 7(j)–7(l). This contrasts with high-energy van Hove singularities which do not appear to form a single peak as  $\theta \rightarrow 0$  but instead a “van Hove comb” of singularities [see Fig. 7(i)].

So far we have considered only the DOS, and we now turn to the nature of the twist bilayer wave functions, and in particular how they differ from SLG wave functions. We shall consider in detail the bilayer system with  $\theta = 0.46^\circ$  [in Fig. 7(r)], but similar results are found for any small-angle case. In Figs. 9(a) and 9(b) is shown  $|\Psi(\mathbf{r})|^2$  integrated over all states in the low-energy peak and the first negative energy satellite, respectively. In the former case we see clear localization on the AA regions of the moiré, while in contrast states in the satellite are entirely expelled from the AB region. In both cases we see a strong localization that can clearly be connected to the moiré geometry (see also Ref. 7). This low-energy localization has been noted in a number of recent works,<sup>7,16</sup> and in particular in Ref. 16 it was shown by calculation of graphene twist *flakes* that a *single moiré unit cell* is sufficient to cause low-energy localization of the quasiparticles. Such behavior is reminiscent of localization by a “moiré quantum well.”

Turning to states at energies far from the Dirac point, we find two quite distinct classes of twist bilayer wave functions: states with an irregular localized appearance, as shown in Fig. 9(c), and SLG type states, see Fig. 9(d) for a representative example; the corresponding eigenvalues are  $\epsilon = -0.503$  eV

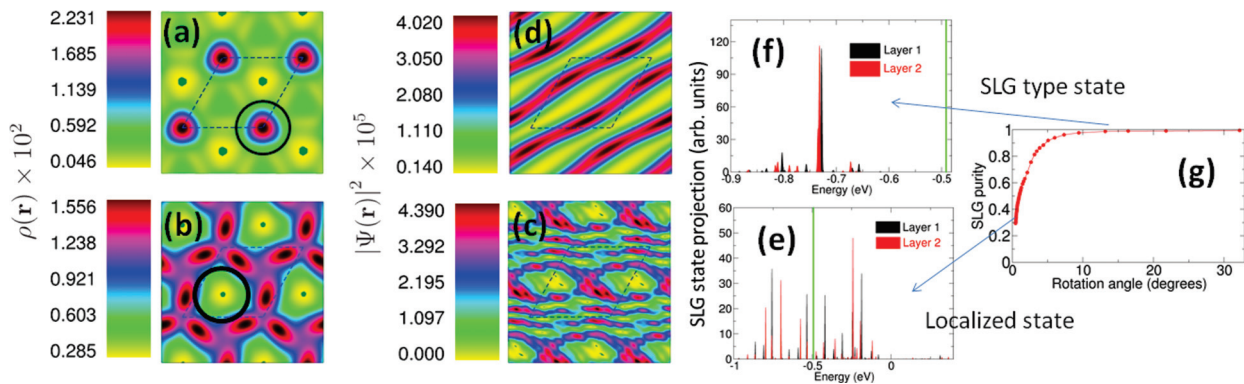


FIG. 9. (Color online)  $\rho(\mathbf{r}) = \sum_i |\Psi_i(\mathbf{r})|^2$  where  $i$  runs over all states in the zero-energy peak in the DOS shown in panel R of Fig. 7 [panel (a)] and over all states in the first neighboring negative energy peak [panel (b)]. Dashed lines indicate twist bilayer unit cell, circles [panels (a) and (b)] indicate regions of AA and AB stacking. Panels (c) and (d) show  $|\Psi_i(\mathbf{r})|^2$  plotted for two eigenstates of energy  $-0.503$  eV and  $-0.512$  eV respectively; the panels on the right-hand side (e) and (f) show the spectrum projected onto the complete set of SLG states. Note that  $\rho(\mathbf{r})$  and  $|\Psi_i(\mathbf{r})|^2$  are shown only in layer 1; results for layer 2 are similar. Panel (g) displays the average SLG purity of the twist bilayer system as a function of rotation angle. As the angle is lowered an increasing number of states are of type (e): localized and consisting of a mix of many SLG states.

and  $\epsilon = -0.512$  eV, respectively. Projecting these states onto the (complete) set of SLG eigenstate states that constitute the basis in our calculations [see Fig. 9(e) and 9(f)], we find that while the states of localized appearance result from the mixing of *many SLG states*, the SLG type states are, as expected, dominated by a SLG eigenstates from a single energy.

To quantify this degree of mixing of SLG states, that evidently occurs at all energies, we define the *SLG purity*  $\gamma_{i\mathbf{k}}$  of a given twist bilayer eigenstate as the sum of the *maximum weight* of the contributing SLG eigenstates in each layer, i.e.,  $\gamma_{i\mathbf{k}} = \max\{|\langle\phi_{i\mathbf{k}_1}^{(1)}|\Psi_{i\mathbf{k}}\rangle|^2\} + \max\{|\langle\phi_{i\mathbf{k}_2}^{(2)}|\Psi_{i\mathbf{k}}\rangle|^2\}$ . For the case of the SLG type wave functions this number is evidently close to 1, while for the states of localized appearance, as shown in Fig. 9(c) and 9(e), this number is much smaller. We then average  $\gamma_{i\mathbf{k}}$  over *all states* in the energy window  $[-0.65, 0.65]$  eV to arrive at a measure of the mixing for a given twist bilayer system. This is plotted in Fig. 9(g) as a function of rotation angle. Clearly, while for  $\theta > 15^\circ$  almost all states are SLG type, indicating that the layers are genuinely decoupled, as  $\theta \rightarrow 0$  and, hence, as the coupling scale  $g^{(c)} \rightarrow 0$ , an increasing number of SLG states are coupled and thus mix, with the consequence of increasing appearance of localization at *all energies*. This “mixing out” of the SLG states we believe is the origin of the “missing” (i.e., non current-carrying) states in recent quantum Hall measurements;<sup>15</sup> the regular nature of the decrease in SLG purity suggests the number of such missing states could provide a reliable measure of the rotation angle.

## V. CONCLUSIONS

To conclude we have shown that the graphene twist bilayer is characterized by an emergent momentum scale  $g^{(c)}$  leading to *effective* reciprocal lattice vectors and Brillouin zone, in general differing from the *geometric* reciprocal lattice vectors and Brillouin zone. In the small-angle limit these are just the reciprocal lattice vectors corresponding to the real-space moiré geometry, although they determine the coupling of states at all angles. We stress that this momentum scale requires no approximation, such as a continuum approximation, in its derivation. This insight leads to a numerical approach that we find to be, in the small-angle regime, several orders of magnitude faster than a direct tight binding approach but with no loss of accuracy. The efficiency of this method is based on (i) the fact that the twist bilayer Hamiltonian takes on an exceptionally sparse structure when expressed in a basis of single-layer graphene states (at  $\theta = 2^\circ$  only  $10^{-4}$  of the matrix elements are typically nonzero) and (ii) the solution of a trivial Diophantine problem (Bézout’s identity) allows one to know which matrix elements assume nonzero value.

With this method we have explored the electronic structure of the twist bilayer as a function of angle, in particular focusing on the density of states and bilayer wave functions. We find a series of both high-energy and low-energy van Hove singularities that, however, are governed by the same underlying momentum scale,  $g^{(c)}$ . The small-angle limit of the twist bilayer is characterized by an increasing number of states being composed of multiple single-layer graphene states, as opposed to the large-angle limit when the twist bilayer wave functions are essentially pure SLG states. Such interference of multiple SLG states leads to the appearance of localization of

the twist bilayer wave function in real space. Interestingly, the fact that the coupling of SLG states on the momentum scale  $g^{(c)}$  plays a critical role in the physics described here implies that manipulating the position of the Dirac cones, as is easy to do by use of an external field, will allow both the Van Hove singularities and state localization to be tuned by such external fields.

In summary, we have presented a complete survey of the twist bilayer system, made possible by a numerical method equivalent to, but several orders of magnitude faster than, standard tight-binding calculations and based on the physical insight of an angle-dependent momentum scale in this system.

## ACKNOWLEDGMENTS

This work was supported by the European Science Foundation under the EUROCORES Program CRP Graphic-9F (DFG Grant No. PA 516/8-1), by the Special Priority Program “Graphene” (DFG Grant No. PA 516/9-1), and by the Collaborative Research Center SFB 953.

## APPENDIX: NUMERICAL SOLUTION OF INTERLAYER MOMENTUM CONSERVATION EQUATION

In this Appendix we shall prove that the equation for the interlayer momentum conservation in the twist bilayer, namely

$$\mathbf{G}_1 = \mathbf{R}\mathbf{G}_2 + (\mathbf{k}_2 - \mathbf{k}_1), \quad (\text{A1})$$

has a lattice of solutions that for *all*  $(\mathbf{k}_2 - \mathbf{k}_1)$  are the given by the *same* reciprocal space commensuration lattice but with *different* shifts off the origin  $\Delta\mathbf{G}$ . Furthermore, we present a numerical method that yields solutions of Eq. (A1) for any  $(\mathbf{k}_2 - \mathbf{k}_1)$ . In Ref. 5 analytical solutions to this equation for a restricted set of  $(\mathbf{k}_2 - \mathbf{k}_1)$  were obtained, and our method here follows closely that used to find these analytical solutions.

Equation (A1) may be visualized as the set of coincident points between two periodic lattices: the reciprocal lattice of single-layer graphene,  $\mathbf{G}_1 = m_1\mathbf{b}_1 + m_2\mathbf{b}_2$ , and the reciprocal lattice of a rotated single-layer graphene layer,  $\mathbf{R}\mathbf{G}_2 = n_1\mathbf{R}\mathbf{b}_1 + n_2\mathbf{R}\mathbf{b}_2$ , but with an additional shift given by  $\mathbf{k}_2 - \mathbf{k}_1$ . See Fig. 1 for an illustration of this. Intuitively, then, if there are solutions at all to Eq. (A1), then these will be of the form of an infinite lattice of solutions  $\{\mathbf{G}_1\}$ .

We first express all the objects in Eq. (A1) in coordinates of the reciprocal lattice of unrotated graphene (we shall refer to this as the *U* coordinate system) and to this end write  $\mathbf{G}_1 = m_1\mathbf{b}_1 + m_2\mathbf{b}_2$  and  $\mathbf{G}_2 = n_1\mathbf{b}_1 + n_2\mathbf{b}_2$ , with  $\mathbf{b}_{1,2}$  the reciprocal lattice vectors of the unrotated graphene lattice. Due to the folding back procedure, see Sec. II, the shift term must always be integer valued in terms of the reciprocal lattice vectors of twist bilayer graphene, and it is thus convenient to express this term as  $\mathbf{k}_2 - \mathbf{k}_1 = l_1\mathbf{g}_1 + l_2\mathbf{g}_2$ , where  $\mathbf{g}_{1,2}$  are the reciprocal lattice vectors of the twist bilayer, defined in Eqs. (6) and (7), and  $l_{1,2}$  are integers. To complete our goal we require that the (right-handed) rotation operator  $\mathbf{R}$  is expressed in *U* coordinates and further require a transformation to take the shift term  $(l_1, l_2)$  to *U* coordinates. For the rotation operator we find

$$\mathbf{R} = \frac{1}{i_3} \begin{pmatrix} i_2 + i_1 & -2i_1 \\ 2i_1 & i_2 - i_1 \end{pmatrix}, \quad (\text{A2})$$

and for the transformation from bilayer to unrotated reciprocal lattice coordinates

$$\mathbf{T}_{\text{BU}} = \frac{\gamma}{i_3} \begin{pmatrix} -p+q & -2q \\ 2q & -p-q \end{pmatrix} \quad (\text{A3})$$

for the case in which  $\delta = 3/\text{gcd}(p,3) = 3$ . We will treat only this case explicitly here; the corresponding derivation for  $\delta = 1$  proceeds in an entirely analogous manner. In Eqs. (A2) and (A3)  $(p,q)$  are a (co-prime) integer pair that label the real-space commensuration, and  $i_{1,2,3}$  are defined by

$$i_1 = 2pq, \quad i_2 = 3q^2 - p^2, \quad i_3 = 3q^2 + p^2. \quad (\text{A4})$$

For details on the derivation of the rotation operator  $\mathbf{R}$  in  $U$  coordinates we refer the reader to Ref. 5, while  $\mathbf{T}_{\text{BU}}$  may be obtained directly from the twist bilayer reciprocal lattice vectors  $\mathbf{g}_{1,2}$ . With these results we are now in a position to write Eq. (A1) in  $U$  coordinates and find

$$\begin{pmatrix} m_1 \\ m_2 \end{pmatrix} = \frac{1}{i_3} \begin{pmatrix} i_2 + i_1 & -2i_1 \\ 2i_1 & i_2 - i_1 \end{pmatrix} \begin{pmatrix} n_1 \\ n_2 \end{pmatrix} + \frac{\gamma}{i_3} \begin{pmatrix} -p+q & -2q \\ 2q & -p-q \end{pmatrix} \begin{pmatrix} l_1 \\ l_2 \end{pmatrix}. \quad (\text{A5})$$

Noting that both the rotation operator  $\mathbf{R}$  and the transformation  $\mathbf{T}_{\text{BU}}$  may be simultaneously diagonalized, we find that Eq. (A5) may be brought to the form

$$\begin{aligned} (m_2 + n_2)p &= (n_3 - m_3)q - \gamma l_2 \\ (n_3 + m_3)p &= (m_2 - n_2)3q - \gamma(2l_1 - l_2), \end{aligned} \quad (\text{A6})$$

where we have introduced  $n_3 = 2n_1 - n_2$  and  $m_3 = 2m_1 - m_2$ . To arrive at this result we diagonalize Eq. (A5) and equate the real and imaginary parts of the resulting formula. We now introduce, without change, two further integers  $a_{1,2}$  into Eq. (A6):

$$\begin{aligned} (m_2 + n_2 - a_1)p &= (n_3 - m_3)q - a_1p - \gamma l_2 \\ (n_3 + m_3 - a_2)p &= (m_2 - n_2)3q - a_2p - \gamma(2l_1 - l_2). \end{aligned} \quad (\text{A7})$$

If we now suppose that there exist  $b_{1,2}$  such that

$$\begin{aligned} -b_1q - a_1p &= -\gamma l_2 \\ -b_23q - a_2p &= -\gamma(2l_1 - l_2), \end{aligned} \quad (\text{A8})$$

we then find that Eq. (A7) takes the form of a homogeneous Diophantine problem for  $(p,q)$

$$\begin{aligned} (m_2 + n_2 - a_1)p &= (n_3 - m_3 - b_1)q \\ (n_2 + m_3 - a_2)p &= (m_2 - n_2 - b_2)3q. \end{aligned} \quad (\text{A9})$$

This equation may evidently be solved by setting  $(m_2 + n_2 - a_1) = sq$ ,  $(n_3 - m_3 - b_1) = sp$ ,  $(n_2 + m_3 - a_2) = 3tq$ , and  $(m_2 - n_2 - b_2) = tp$  where  $s,t$  are integers and then solving to find  $m_{1,2}$  and  $n_{1,2}$ . After some algebra we find for  $m_{1,2}$

$$\begin{pmatrix} m_1 \\ m_2 \end{pmatrix} = \alpha \frac{1}{\gamma} \begin{pmatrix} -p+q \\ 2q \end{pmatrix} + \beta \frac{1}{\gamma} \begin{pmatrix} 2q \\ p+q \end{pmatrix} + \frac{1}{4} \begin{bmatrix} a_1 + a_2 - b_1 + b_2 \\ 2(a_1 + b_2) \end{bmatrix}, \quad (\text{A10})$$

where  $\alpha, \beta$  are arbitrary integers and the parameter  $\gamma = \text{gcd}(3q+q, 3q-p)$  is introduced to ensure that noninteger  $\alpha, \beta$  cannot yield integer  $m_{1,2}$ .<sup>5</sup> We thus see that the solutions of Eq. (A1) are given by a lattice of points for which the primitive vectors are  $(-p+q)/\gamma \mathbf{b}_1 + 2q/\gamma \mathbf{b}_2$  and  $2q/\gamma \mathbf{b}_1 + (p+q)/\gamma \mathbf{b}_2$ . As these primitive vectors are independent of  $l_{1,2}$ , and, thus, independent of  $\mathbf{k}_2 - \mathbf{k}_1$ , we see that for *all*  $\mathbf{k}_2 - \mathbf{k}_1$  the solutions of Eq. (A1) describe the *same* lattice of solutions, but with a shift off the origin given by the last term in Eq. (A10). This is what we wished to prove.

All that now remains is to find a numerical solution this shift term, i.e., for  $a_{1,2}$  and  $b_{1,2}$ . This may be achieved by noting that Eq. (A8) represents two separate linear Diophantine problems for which the solution can easily be found numerically. We recall that the linear Diophantine problem  $ax + by = c$  (also known as Bézout's identity), where  $a, b$ , and  $c$  are all integers and we require integer solutions  $x$  and  $y$ , has (i) no solution if  $\text{gcd}(a,b)$  is not a divisor of  $c$  and (ii) an infinite set of solutions  $x = b/\text{gcd}(a,b)k + x_0$  and  $y = -a/\text{gcd}(a,b)j + y_0$  if  $\text{gcd}(a,b)$  is a divisor of  $c$ . The values of  $x_0, y_0$  cannot generally be obtained analytically but may be found via the extended Euclid algorithm.<sup>20</sup> Using the fact that  $\text{gcd}(p,q) = 1$  by construction, and that as  $\delta = 3/\text{gcd}(p,3) = 3$ , then 3 is not a divisor of  $p$  and, thus, in addition, we have  $\text{gcd}(p,3q) = 1$ , the solution to Eq. (A8) is

$$\begin{aligned} a_1 &= -qk + a_1^{(0)} & b_1 &= -pk + b_1^{(0)} \\ a_2 &= -3qj + a_2^{(0)} & b_2 &= -pj + b_2^{(0)}, \end{aligned} \quad (\text{A11})$$

where  $a_{1,2}^{(0)}$  and  $b_{1,2}^{(0)}$  must be obtained by the extended Euclid algorithm and  $k, j$  are integers. From Eq. (A11) we find that

$$\begin{aligned} \frac{1}{4} \begin{pmatrix} a_1 + a_2 - b_1 + b_2 \\ 2(a_1 + b_2) \end{pmatrix} &= -\frac{1}{\gamma} \begin{pmatrix} k \\ j \end{pmatrix} \begin{pmatrix} -p+q \\ 2q \end{pmatrix} \\ &\quad - \frac{1}{\gamma} \begin{pmatrix} k \\ j \end{pmatrix} \begin{pmatrix} -p+q \\ 2q \end{pmatrix} \\ &\quad + \frac{1}{4} \begin{pmatrix} a_1^{(0)} + a_2^{(0)} - b_1^{(0)} + b_2^{(0)} \\ 2(a_1^{(0)} + b_2^{(0)}) \end{pmatrix} \end{aligned} \quad (\text{A12})$$

and so the terms depending on  $k, j$  lead only to the homogeneous part of Eq. (A10). The shift term  $\Delta \mathbf{G}$  that we seek is, thus, given by

$$\Delta \mathbf{G} = (a_1^{(0)} + a_2^{(0)} - b_1^{(0)} + b_2^{(0)}) \mathbf{b}_1 + 2(a_1^{(0)} + b_2^{(0)}) \mathbf{b}_2. \quad (\text{A13})$$

Finally, we note that there exists one circumstance in which Eq. (A8) may be solved analytically: when  $l_{1,2} = 2p/\gamma n_{1,2}$  with the  $n_{1,2}$  integer. In this case, the terms on the right-hand side may be absorbed into the prefactor of  $p$  on the left-hand side, and the resulting pair of equations solved in exactly the manner as in Eq. (A9). This approach leads to the analytical results quoted in Sec. II and first derived in another way in Ref. 5.

\*phsss@tfkp.physik.uni-erlangen.de

- <sup>1</sup>J. M. B. Lopes dos Santos, N. M. R. Peres, and A. H. Castro Neto, *Phys. Rev. Lett.* **99**, 256802, (2007).
- <sup>2</sup>J. Hass, F. Varchon, J. E. Millán-Otoya, M. Sprinkle, N. Sharma, W. A. de Heer, C. Berger, P. N. First, L. Magaud, and E. H. Conrad, *Phys. Rev. Lett.* **100**, 125504 (2008).
- <sup>3</sup>S. Shallcross, S. Sharma, and O. A. Pankratov, *Phys. Rev. Lett.* **101**, 056803 (2008).
- <sup>4</sup>Guohong Li *et al.*, *Nat. Phys.* **6**, 109 (2010).
- <sup>5</sup>S. Shallcross, S. Sharma, E. Kandelaki, and O. A. Pankratov, *Phys. Rev. B* **81**, 165105 (2010).
- <sup>6</sup>E. J. Mele, *Phys. Rev. B* **81**, 161405(R) (2010).
- <sup>7</sup>Guy Trambly de Laissardière, Didier Mayou, and Laurence Magaud, *Nano Lett.* **10**, 804 (2010).
- <sup>8</sup>R. Bistritzer and A. H. MacDonald, *Proc. Natl Acad. Sci. USA* **108**, 12233 (2010).
- <sup>9</sup>M. Kindermann and P. N. First, *Phys. Rev. B* **83**, 045425 (2011).
- <sup>10</sup>Min-Young Choi, Young-Hwan Hyun, and Yoonbai Kim, *Phys. Rev. B* **84**, 195437 (2011).
- <sup>11</sup>E. Suárez Morell, P. Vargas, L. Chico, and L. Brey, *Phys. Rev. B* **84**, 195421 (2011).
- <sup>12</sup>A. Luican, G. Li, A. Reina, J. Kong, R. R. Nair, K. S. Novoselov, A. K. Geim, and E. Y. Andrei, *Phys. Rev. Lett.* **106**, 126802 (2011).
- <sup>13</sup>E. J. Mele, *J. Phys. D: Appl. Phys.* **45**, 154004 (2012).
- <sup>14</sup>P. San-Jose, J. González, and F. Guinea, *Phys. Rev. Lett.* **108**, 216802 (2012).
- <sup>15</sup>Dong Su Lee, Christian Riedl, Thomas Beringer, A. H. Castro Neto, Klaus von Klitzing, Ulrich Starke, and Jurgen H. Smet, *Phys. Rev. Lett.* **107**, 216602 (2011).
- <sup>16</sup>W. Landgraf, S. Shallcross, K. Türschmann, D. Weckbecker, and O. Pankratov, *Phys. Rev. B* **87**, 075433 (2013).
- <sup>17</sup>This type of effective Brillouin zone is well known in the semiconductor literature where it goes by the name of a *Jones zone*; see W. A. Harrison, *Solid State Theory* (Dover, London, 1979).
- <sup>18</sup>[<http://www.caam.rice.edu/software/ARPACK/>].
- <sup>19</sup>G Lamé, *Comptes Rendus Acad. Sci.* **19**, 867 (1844).
- <sup>20</sup>Jorn Steuding, *Diophantine Analysis* (Chapman & Hall/CRC, London, 2005).